

Measuring $\mathcal{B}(D^+ \rightarrow \mu^+ \nu)$ and the pseudoscalar decay constant f_{D^+}

G. Bonvicini, D. Cinabro, and M. Dubrovin
Wayne State University, Detroit, Michigan 48202, USA

J. L. Rosner
Enrico Fermi Institute, University of Chicago, Chicago, Illinois 60637, USA

R. A. Briere, G. P. Chen, T. Ferguson, G. Tatishvili, H. Vogel, and M. E. Watkins
Carnegie Mellon University, Pittsburgh, Pennsylvania 15213, USA

N. E. Adam, J. P. Alexander, K. Berkelman, D. G. Cassel, V. Crede, J. E. Duboscq, K. M. Ecklund, R. Ehrlich, L. Fields, R. S. Galik, L. Gibbons, B. Gittelman, R. Gray, S. W. Gray, D. L. Hartill, B. K. Heltsley, D. Hertz, L. Hsu, C. D. Jones, J. Kandaswamy, D. L. Kreinick, V. E. Kuznetsov, H. Mahlke-Krüger, T. O. Meyer, P. U. E. Onyisi, J. R. Patterson, D. Peterson, J. Pivarski, D. Riley, A. Ryd, A. J. Sadoff, H. Schwarthoff, M. R. Shepherd, S. Stroiney, W. M. Sun, J. G. Thayer, D. Urner, T. Wilksen, and M. Weinberger
Cornell University, Ithaca, New York 14853, USA

S. B. Athar, P. Avery, L. Bрева-Newell, R. Patel, V. Potlia, H. Stoeck, and J. Yelton
University of Florida, Gainesville, Florida 32611, USA

P. Rubin
George Mason University, Fairfax, Virginia 22030, USA

C. Cawfield, B. I. Eisenstein, G. D. Gollin, I. Karliner, D. Kim, N. Lowrey, P. Naik, C. Sedlack, M. Selen, J. J. Thaler, J. Williams, and J. Wiss
University of Illinois, Urbana-Champaign, Illinois 61801, USA

K. W. Edwards
Carleton University, Ottawa, Ontario, Canada K1S 5B6, and the Institute of Particle Physics, Canada

D. Besson
University of Kansas, Lawrence, Kansas 66045, USA

T. K. Pedlar
Luther College, Decorah, Iowa 52101, USA

D. Cronin-Hennessy, K. Y. Gao, D. T. Gong, Y. Kubota, B. W. Lang, S. Z. Li, R. Poling, A. W. Scott, A. Smith, and C. J. Stepaniak
University of Minnesota, Minneapolis, Minnesota 55455, USA

S. Dobbs, Z. Metreveli, K. K. Seth, A. Tomaradze, and P. Zweber
Northwestern University, Evanston, Illinois 60208, USA

J. Ernst and A. H. Mahmood
State University of New York at Albany, Albany, New York 12222, USA

H. Severini
University of Oklahoma, Norman, Oklahoma 73019, USA

D. M. Asner, S. A. Dytman, W. Love, S. Mehrabyan, J. A. Mueller, and V. Savinov
University of Pittsburgh, Pittsburgh, Pennsylvania 15260, USA

Z. Li, A. Lopez, H. Mendez, and J. Ramirez
University of Puerto Rico, Mayaguez, Puerto Rico 00681

G. S. Huang, D. H. Miller, V. Pavlunin, B. Sanghi, E. I. Shibata, and I. P. J. Shipsey
Purdue University, West Lafayette, Indiana 47907, USA

G. S. Adams, M. Chasse, M. Cravey, J. P. Cummings, I. Danko, and J. Napolitano
Rensselaer Polytechnic Institute, Troy, New York 12180

C. S. Park, W. Park, J. B. Thayer, and E. H. Thorndike
University of Rochester, Rochester, New York 14627, USA

T. E. Coan, Y. S. Gao, and F. Liu
Southern Methodist University, Dallas, Texas 75275, USA

M. Artuso, C. Boulahouache, S. Blusk, J. Butt, E. Dambasuren, O. Dorjkhaidav, J. Li, N. Menea, R. Mountain,
 H. Muramatsu, R. Nandakumar, R. Redjimi, R. Sia, T. Skwarnicki, S. Stone, J. C. Wang, and K. Zhang
Syracuse University, Syracuse, New York 13244, USA

S. E. Csorna
Vanderbilt University, Nashville, Tennessee 37235, USA

(CLEO Collaboration)

(Received 11 November 2004; published 17 December 2004)

In 60 pb⁻¹ of data taken on the $\psi(3770)$ resonance with the CLEO-c detector, we find eight $D^+ \rightarrow \mu^+ \nu$ decay candidates that are mostly signal, containing only one estimated background. Using this statistically compelling sample, we measure a value of $\mathcal{B}(D^+ \rightarrow \mu^+ \nu) = (3.5 \pm 1.4 \pm 0.6) \times 10^{-4}$, and determine $f_{D^+} = (202 \pm 41 \pm 17)$ MeV.

DOI: 10.1103/PhysRevD.70.112004

PACS numbers: 13.20.Fc, 13.66.Bc

I. INTRODUCTION

Measuring purely leptonic decays of heavy mesons allows the determination of meson decay constants, which connect measured quantities, such as the $B\bar{B}$ mixing ratio, to Cabibbo-Kobayashi-Maskawa (CKM) matrix elements. Currently, it is not possible to determine f_B experimentally from leptonic B decays, so theoretical calculations of f_B must be used. The most promising of these calculations involves lattice QCD [1–3], though there are other methods [4–8].

Measurements of pseudoscalar decay constants such as f_{D^+} provide checks on these calculations and help discriminate among different models.

The decay diagram for $D^+ \rightarrow \mu^+ \nu$ is shown in Fig. 1. The decay rate is given by [9]

$$\Gamma(D^+ \rightarrow \ell^+ \nu) = \frac{G_F^2}{8\pi} f_{D^+}^2 m_\ell^2 M_{D^+} \left(1 - \frac{m_\ell^2}{M_{D^+}^2}\right)^2 |V_{cd}|^2, \quad (1)$$

where M_{D^+} is the D^+ mass, m_ℓ is the mass of the final state lepton, V_{cd} is a CKM matrix element equal to 0.224 [10], and G_F is the Fermi coupling constant. Various theoretical predictions of f_{D^+} range from 190 to 350 MeV [1–8]. Because of helicity suppression, the electron mode $D^+ \rightarrow e^+ \nu$ has a very small rate in the Standard Model [11]. The relative widths are 2.64:1:2.3 $\times 10^{-5}$ for the $\tau^+ \nu$, $\mu^+ \nu$ and $e^+ \nu$ final states, respectively. Unfortunately the mode with the largest branching fraction, $\tau^+ \nu$, has at least two neutrinos in the final state and is difficult to detect.

II. THE CLEO-C DETECTOR

The CLEO-c detector is equipped to measure the momenta and direction of charged particles, identify charged hadrons, detect photons, and determine with good precision their directions and energies. Muons above 1.1 GeV can also be identified. The detector is almost cylindrically symmetric with everything but the muon detector inside a superconducting magnet coil run at a current that produces an almost uniform 1.0 T field. The detector consists of a six-layer wire drift chamber at small radius that is low mass, suitable for these relatively low energies. It is followed by a 47-layer drift chamber; both chambers use a gas mixture of 60% helium and 40% propane. These two devices measure charged track three-momenta with excellent accuracy. The drift chamber also measures energy loss, dE/dx , that is used to identify charged tracks below about 0.7 GeV [12]. After the drift chamber there is a Ring

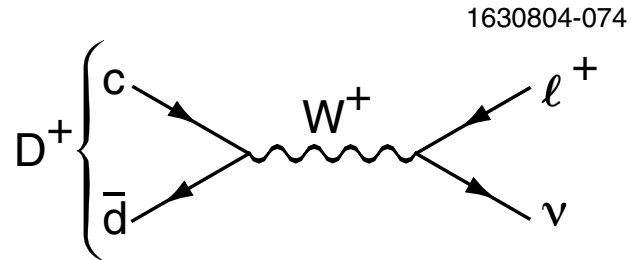


FIG. 1. The decay diagram for $D^+ \rightarrow \mu^+ \nu$.

Imaging Cherenkov Detector (RICH) [13], that identifies charged particles over most of their momentum range. The RICH is surrounded by a thallium doped CsI crystal array consisting of about 8000 tapered crystals, 30 cm long and about $5 \times 5 \text{ cm}^2$ at the front [14].

III. DATA SAMPLE AND SIGNAL SELECTION

In this study we use 60 pb^{-1} of CLEO-c data produced in e^+e^- collisions and recorded at the ψ'' resonance (3.770 GeV). At this energy, the events consist of a mixture of pure D^+D^- , $D^0\bar{D}^0$ three-flavor continuum, and $\gamma\psi$ events. There also may be small amounts of $\tau^+\tau^-$ pairs and two-photon events.

We examine all the recorded events and retain those containing at least one charged D candidate in the modes listed in Table I. The selection criteria are described in detail in what follows. We then use this sample to look for cases where we have only a single muon candidate whose four-momentum is consistent with a two-body D decay into a muon and a neutrino and no other charged tracks or excess neutral energy are present.

All acceptable track candidates must have a helical trajectory that approaches the event origin within a distance of 5 mm in the azimuthal projection and 5 cm in the polar view, where the azimuthal projection is in the bend view of the solenoidal magnet. Each track must possess at least 50% of the hits expected to be on a track, and it must be within the fiducial volume of the drift chambers, $|\cos\theta| < 0.93$, where θ is the polar angle with respect to the beam direction.

We use both charged particle ionization loss in the drift chamber (dE/dx) and RICH information to identify kaons and pions used to fully reconstruct D mesons. The RICH is used for momenta larger than 0.55 GeV. Information on the angle of detected Cherenkov photons is translated into a likelihood of a given photon being due to a particular particle. Contributions from all photons associated with a particular track are then summed to form an overall likelihood denoted as \mathcal{L}_i for each particle hypothesis. To differentiate between pion and kaon candidates, we use the difference: $-2\log(\mathcal{L}_\pi) + 2\log(\mathcal{L}_K)$. Usually this cut is set at zero except for muon candidates where the difference $-2\log(\mathcal{L}_\mu) + 2\log(\mathcal{L}_K)$ is required to be less than

10, to ensure a high, well understood efficiency. To utilize the dE/dx information we calculate σ_π as the difference between the expected ionization loss for a pion and the measured loss divided by the measurement error. Similarly, σ_K is defined in the same manner using the expected ionization for a kaon.

We use both the RICH and dE/dx information for D^- meson tag candidate tracks in the following manner: (a) If neither the RICH nor dE/dx information is available, then the track is accepted as both a pion and a kaon candidate. (b) If dE/dx is available and RICH is not then we insist that pion candidates have $PID_{dE} \equiv \sigma_\pi^2 - \sigma_K^2 < 0$, and kaon candidates have $PID_{dE} > 0$. (c) If RICH information is available and dE/dx is not available, then we require that $PID_{\text{RICH}} \equiv -2\log(\mathcal{L}_\pi) + 2\log(\mathcal{L}_K) < 0$ for pions and $PID_{\text{RICH}} > 0$ for kaons. (d) If both dE/dx and RICH information are available, we require that $(PID_{dE} + PID_{\text{RICH}}) < 0$ for pions and $(PID_{dE} + PID_{\text{RICH}}) > 0$ for kaons.

We reconstruct π^0 's by first selecting photon candidates from energy deposits in the crystals not matched to charged tracks that have deposition patterns consistent with that expected for electromagnetic showers. Pairs of photon candidates are kinematically fit to the known π^0 mass. We require the pull, the difference between the raw and fit mass normalized by its uncertainty, to be less than three for acceptable π^0 candidates.

K_S candidates are formed from a pair of charged pions which are constrained to come from a single vertex. We also require that the invariant mass of the two pions be within 4.5 times the width of the K_S mass peak, which has an rms width of 4 MeV.

IV. RECONSTRUCTION OF CHARGED D TAGGING MODES

Tagging modes are fully reconstructed by first evaluating the difference in the energy, ΔE , of the decay products with the beam energy. We then require the absolute value of this difference to be within 20 MeV of zero, approximately twice the rms width, and then look at the reconstructed D^- beam-constrained mass defined as

$$m_D = \sqrt{E_{\text{beam}}^2 - \left(\sum_i \vec{p}_i\right)^2}, \quad (2)$$

where i runs over all the final state particles. The beam-constrained mass has better resolution than merely calculating the invariant mass of the decay products since the beam has a small energy spread. Besides using D^- tags and searching for $D^+ \rightarrow \mu^+ \nu$, we also use the charge-conjugate D^+ tags and search for $D^- \rightarrow \mu^- \bar{\nu}_\mu$; in the rest of this paper we will not mention the charge-conjugate modes explicitly, but they are always used.

The m_D distributions for all D^- tagging modes considered in this data sample are shown in Fig. 2 and listed in Table I along with the numbers of signal events and back-

TABLE I. Tagging modes and numbers of signal and background events determined from the fits shown in Fig. 2.

Mode	Signal	Background
$K^+ \pi^- \pi^-$	$15\,173 \pm 140$	583
$K^+ \pi^- \pi^- \pi^0$	4082 ± 81	1826
$K_S \pi^-$	2124 ± 52	251
$K_S \pi^- \pi^- \pi^+$	3975 ± 81	1880
$K_S \pi^- \pi^0$	3297 ± 87	4226
Sum	$28\,651 \pm 207$	8765

ground events within ± 3 rms widths of the peak. The event numbers are determined from fits of the m_D distributions to Gaussian signal functions plus a background shape. We fit with two different background parametrizations: (a) a third order polynomial, (b) a shape function analogous to one first used by the ARGUS collaboration [15] which has approximately the correct threshold behavior at large m_D ; to use this function, we first fit it to the data selected by using ΔE sidebands, mode by mode, defined as $40 \text{ MeV} < |\Delta E| < 60 \text{ MeV}$ to fix the shape parameters in each mode allowing the normalization to float. For the $K^+ \pi^- \pi^- \pi^0$, $K_S \pi^- \pi^- \pi^+$ and $K_S \pi^- \pi^0$ modes we use a single Gaussian to describe the signal whose mass and width are allowed to float. For the $K^+ \pi^- \pi^-$ and $K_S \pi^-$ modes, where we see a small tail on the higher mass side, we use the sum of two Gaussians for a signal function [16]; in this case both the means and widths of both Gaussians are allowed to float.

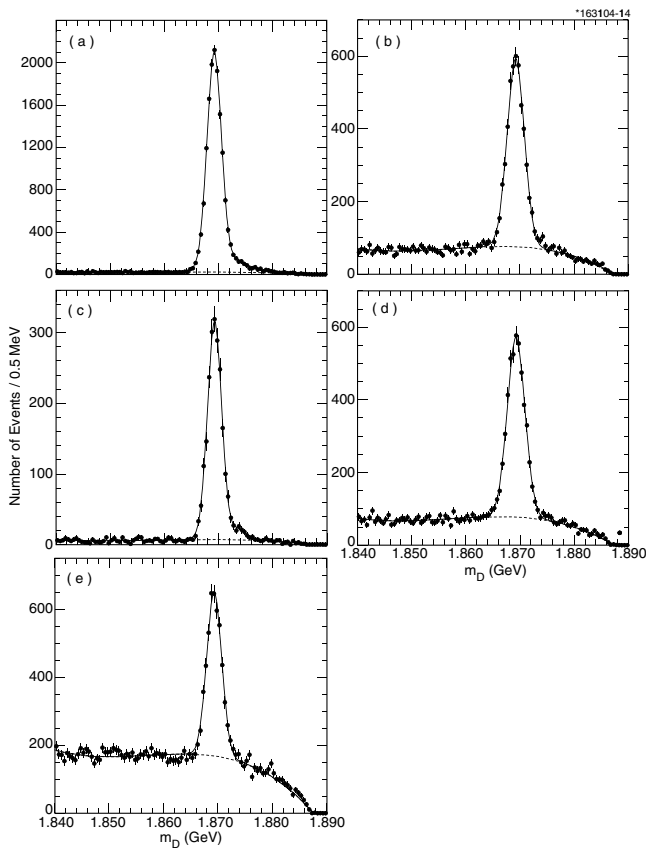


FIG. 2. Beam-constrained mass distributions for different fully reconstructed D^- decay candidates in the modes: (a) $D^- \rightarrow K^+ \pi^- \pi^-$, (b) $D^- \rightarrow K^+ \pi^- \pi^- \pi^0$, (c) $D^- \rightarrow K_S \pi^-$, (d) $D^- \rightarrow K_S \pi^- \pi^- \pi^+$ and (e) $D^- \rightarrow K_S \pi^- \pi^0$. The solid curves show the sum of Gaussian signal functions and third order polynomial background functions. A single signal Gaussian is used for all modes except for modes (a) and (c) where the sum of two Gaussians are used. The dashed curves indicate the background fits.

The difference between using the polynomial and ARGUS shapes in the signal yields is $\pm 2.2\%$, which we use as an estimate of the systematic error.

Selecting those candidates within three rms widths of the D^- mass reduces the signal number by 77 events giving a total of $28\,574 \pm 207 \pm 629$ single tag events that we use for further analysis. In the case of two Gaussians the wider width was used.

V. $D^+ \rightarrow \mu^+ \nu_\mu$ SELECTION CRITERIA

Using our sample of D^- event candidates we search for events with a single additional charged track presumed to be a μ^+ . Then we infer the existence of the neutrino by requiring a measured value near zero (the neutrino mass) of the missing mass squared (MM^2) defined as

$$MM^2 = (E_{\text{beam}} - E_{\mu^+})^2 - (-\vec{p}_{D^-} - \vec{p}_{\mu^+})^2, \quad (3)$$

where \vec{p}_{D^-} is the three-momentum of the fully reconstructed D^- .

We need to restrict the sample to candidate $\mu^+ \nu_\mu$ events resulting from the other D . Thus we wish to exclude events with more than one additional track with opposite charged to the tagged D , which we take to be the muon candidate, or with extra neutral energy. It is possible, in fact even likely, that the decay products of the tagging D^- interact in the detector material, mostly the crystal electromagnetic calorimeter (EM) and spray tracks and neutral energy back into the rest of the detector. To evaluate the size of these contributions we use a very pure sample of events obtained by finding fully reconstructed $D^0 \bar{D}^0$ events. The numbers of these events in various decay modes are listed in Table II, a total of 782 events.

The number of interactions of particles with material and their consequences depend on the number of particles, the kind of particles and their momenta. Thus, the sum over these neutral D decay modes is not quite the same as the sum over the tagging D^- decay; however, after accounting for the differences between the pion-nucleon and kaon-nucleon cross sections and the different momentum distributions of the tracks, we find that the average over these modes is quite similar to the D^- tagging modes for this level of statistics.

Extra tracks do appear in these $D^0 \bar{D}^0$ events. None of these tracks, however, approach the main event vertex. Requiring that good tracks are within 5 cm along the beam and 5 mm perpendicular to the beam does not include any additional tracks from interactions in the material. We

TABLE II. Fully reconstructed $D^0 \bar{D}^0$ events.

Mode one	Mode two	No. of events
$K^- \pi^+$	$K^+ \pi^-$	89
$K^+ \pi^- \pi^+ \pi^-$	$K^- \pi^+$	392
$K^+ \pi^- \pi^+ \pi^-$	$K^- \pi^+ \pi^- \pi^+$	301

also reject D^- tags with additional $K_S \rightarrow \pi^+ \pi^-$ candidates.

In the $D^0 \bar{D}^0$ events, energy in the calorimeter not matched to any of the charged tracks is shown in Fig. 3. Figure 3(a) shows the energy of the largest shower and 3(b) shows the total. We accept only as extra showers those that do not match a charged track within a connected region. A connected region is a group of adjacent crystals with energy depositions which are nearest neighbors. This suppresses hadronic shower fragments which would otherwise show up as unmatched showers. Hadronic interactions and very energetic π^0 's tend to produce one connected region with many clusters. For further analysis we require that the largest unmatched shower not to be larger than 250 MeV. This requirement is $(93.5 \pm 0.9)\%$ efficient for signal events, estimated from the distribution of extra energies in the $D^0 \bar{D}^0$ tag sample. We assign an additional 4% systematic error, due to the difference in our double tag and single tag samples.

The muon candidate is required to be within the barrel region of the detector $|\cos\theta| < 0.81$; this requirement ensures that the MM^2 resolution is good as tracks at larger angles cross fewer tracking layers and consequently are measured with poorer precision. In addition, this requirement helps reject background from the decay $D^+ \rightarrow \pi^+ \pi^0$; this mode also gives a MM^2 near zero. Requiring the muon candidate in the barrel region (the π^+ in this case) avoids having the photons from this decay being lost

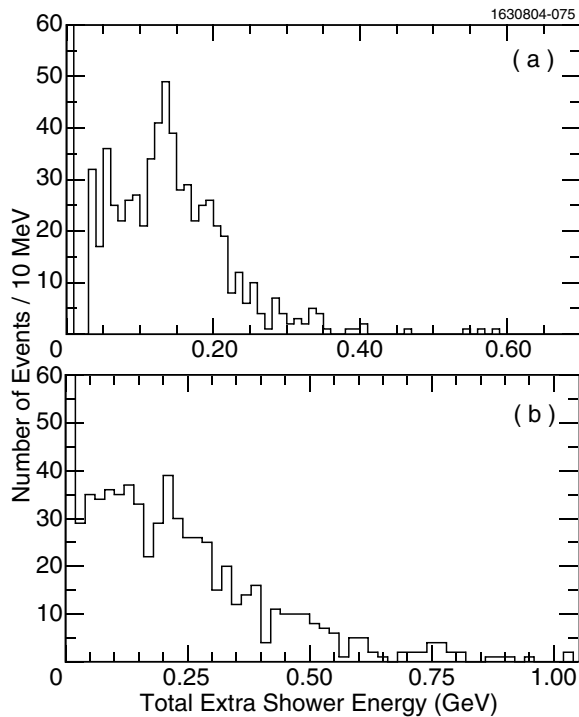


FIG. 3. Largest (a) and total extra shower (b) energies in the $D^0 \bar{D}^0$ sample. In both cases the first bin is truncated; each plot has 782 total entries.

in the transition region of the calorimeter between the barrel and the end cap, because the π^0 direction is almost directly opposite the π^+ . Furthermore, the muon candidate is required not to be consistent with the kaon hypothesis using RICH information. Finally, we also require that the muon candidate deposits less than 300 MeV of energy in the calorimeter, characteristic of a minimum ionizing particle. This requirement is very efficient for real muons, and rejects about 40% of the pions as determined using a sample of reconstructed $D^0 \rightarrow K^- \pi^+$ decays. Figure 4 shows the muon deposited energy in the EM calorimeter both from data on $e^+ e^- \rightarrow \mu^+ \mu^-$ and from GEANT simulation of the same process. The Monte Carlo and data are in excellent agreement for muon shower energies. We therefore use a GEANT simulation of $D^+ \rightarrow \mu^+ \nu$ with lower energy muons to determine that the efficiency of the calorimeter energy cut is $(98.7 \pm 0.2)\%$.

When evaluating MM^2 using Eq. (3) there are two important considerations that are not obvious. First of all, we explicitly need to take into account the crossing angle between the e^+ and e^- beams. This angle is about 4 mrad, varying slightly run to run; we use this information and Lorentz transform all laboratory quantities to the center-of-mass. Second, we change the reconstructed D^- momenta so that they give exactly the known D^- mass; this changes and improves somewhat our knowledge of the D^- direction.

The MM^2 from Monte Carlo simulation is shown for our different tagging samples in Fig. 5. The signal is fit to a sum of two Gaussians with the wider Gaussian having about 30% of the area independent of tagging mode. The resolution (σ) is defined as

$$\sigma = f_1 \sigma_1 + (1 - f_1) \sigma_2, \quad (4)$$

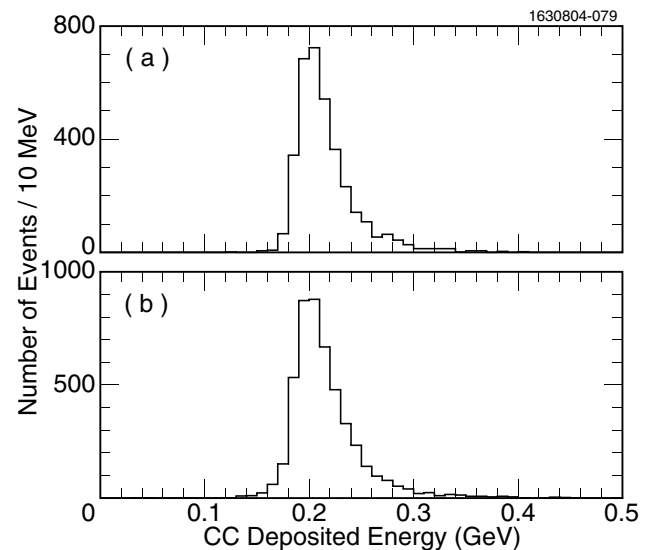


FIG. 4. Deposited energy in the crystal calorimeter of muons created in the process $e^+ e^- \rightarrow \mu^+ \mu^-$ from (a) data and (b) Monte Carlo.

where σ_1 and σ_2 are the individual widths of the two Gaussians and f_1 is the fractional area of the first Gaussian. The resolution is approximately 0.025 GeV^2 consistent among all the tagging decay modes.

We check our simulations using the $D^+ \rightarrow K_S \pi^+$ decay. Here we choose events with the same requirements as used to search for $\mu^+ \nu$ but require one additional found K_S . The MM^2 distribution for this final state is shown in Fig. 6 and peaks as expected at the K_S mass-squared of 0.25 GeV^2 . The resolution is measured to be $0.024 \pm 0.002 \text{ GeV}^2$ from a single Gaussian fit, consistent with but slightly larger than the Monte Carlo estimate of $0.021 \pm 0.001 \text{ GeV}^2$. To account for the difference in resolution between data and simulations we scale the resolution by 14% to 0.028 GeV^2 when looking for the $D^+ \rightarrow \mu^+ \nu_\mu$ signal.

The MM^2 distributions for our tagged events requiring no extra charged tracks besides the muon candidate and showers above 250 MeV as described above is shown in Fig. 7. We see a small signal near zero containing eight events within a 2σ interval, -0.056 to $+0.056 \text{ GeV}^2$. This signal is most likely due to the $D^+ \rightarrow \mu^+ \nu_\mu$ mode we are seeking. The large peak centered near 0.25 GeV^2 is from

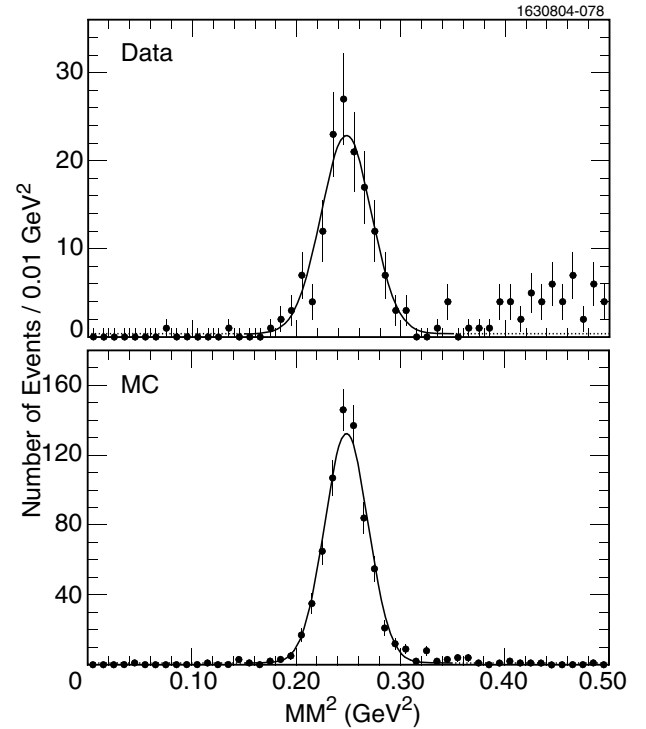


FIG. 6. MM^2 distribution for the decay $D^+ \rightarrow K_S \pi^+$ from data and signal Monte Carlo simulation

the decay $D^+ \rightarrow \bar{K}^0 \pi^+$ that is far from our signal region and is expected since many K_L would escape our detector.

Table III lists the properties of each muon candidate from the eight events in the signal region. A typical event is shown in Fig. 8.

VI. BACKGROUND EVALUATION

A. Introduction

There are several background sources we need to evaluate. These include background from other D^+ modes, background from misidentified $D^0 \bar{D}^0$ events and continuum background. The requirement of the muon depositing $<300 \text{ MeV}$ in the calorimeter, while about 99% efficient on muons, rejects only about 40% of pions as determined from the $D^0 \bar{D}^0$ event sample where the pion from the $K^\pm \pi^\mp$ mode was examined. In Fig. 9 we show the deposited energy in the calorimeter for both kaons and pions obtained from the $K\pi$ tag sample.

B. D^+ backgrounds

There are a few D^+ decay modes that could mimic the signal. These are listed in Table IV along with the background estimate we obtained by Monte Carlo generation and reconstruction of each specific mode. The branching ratios are from the Particle Data Group except for the $\pi^+ \pi^0$ mode where a separate CLEO analysis gives a somewhat lower value [17]. This mode is the most difficult

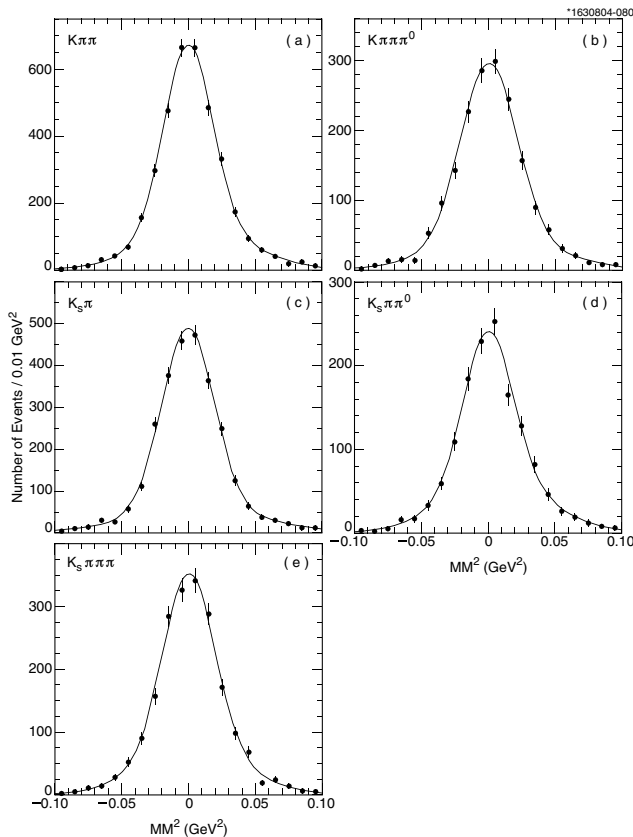


FIG. 5. Monte Carlo simulation of $D^+ \rightarrow \mu^+ \nu_\mu$ events for different tags. The plots have been fitted to two Gaussians centered at zero where the second Gaussian constitutes around 30% of area.

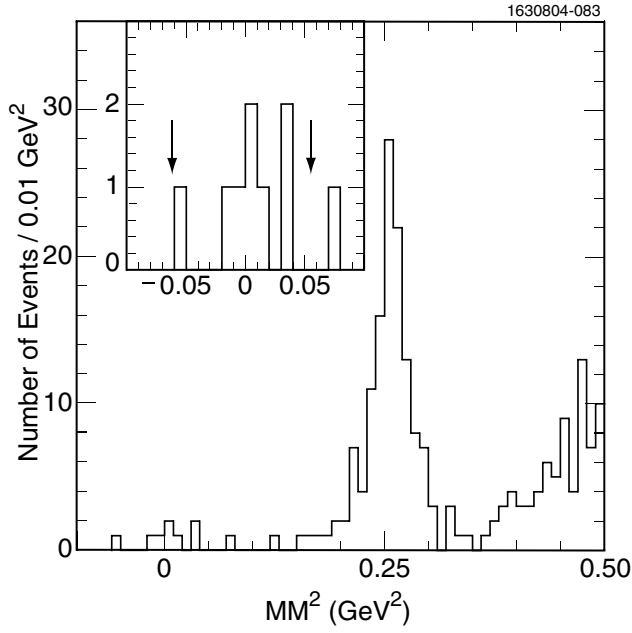


FIG. 7. MM^2 using D^- tags and one additional opposite sign charged track and no extra energetic showers (see text). The inset shows the signal region for $D^+ \rightarrow \mu^+ \nu$ enlarged; the $\pm 2\sigma$ range is shown between the two arrows.

to reject because the MM^2 peaks very close to zero, at 0.018 GeV^2 , well within our resolution of 0.028 GeV^2 . While we have insisted that the muon candidate be well within our acceptance, it is possible for the photons from the π^0 decay to inadvertently be matched to the tracks from the tagging D^- or be missed. The maximum photon energy of the π^0 from a GEANT simulation of $D^+ \rightarrow \pi^+ \pi^0$ is shown in Fig. 10. We note that at least one photon from the $\pi^+ \pi^0$ mode exceeds our 250 MeV calorimeter energy requirement and should in most cases cause such a decay to be vetoed.

Even though the $\bar{K}^0 \pi^+$ mode gives a large peak in the MM^2 spectrum near 0.25 GeV^2 , our simulation shows that only a very small amount can enter our signal region, only

TABLE III. Muon Candidate Properties. (CC indicates the crystal calorimeter.)

Tag	MM^2 (GeV^2)	CC energy of μ^+ (GeV)	$-2 \log(\mathcal{L}_K)$	$-2 \log(\mathcal{L}_\mu)$	μ^\pm
$K \pi \pi \pi^0$	0.032	0.186	-4.3	-166.0	+
$K_S \pi$	-0.019	0.201	0.0	-140.0	-
$K \pi \pi$	-0.051	0.190	31.9	-252.9	+
$K \pi \pi$	-0.004	0.221	0.0	-115.2	+
$K_S \pi \pi^0$	0.032	0.164	-0.3	-130.6	-
$K_S \pi \pi \pi$	0.001	0.245	-11.7	-138.9	+
$K \pi \pi \pi^0$	0.002	0.204	-8.6	-88.6	-
$K_S \pi \pi^0$	0.014	0.208	-8.3	-113.0	+

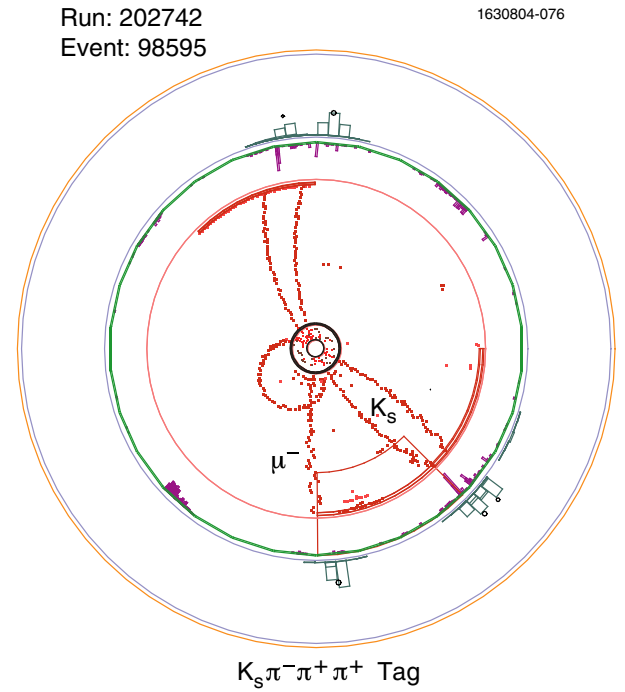


FIG. 8 (color online). A typical $D^- \rightarrow \mu^- \bar{\nu}_\mu$ event. The tag in this case is $D^- \rightarrow K_S \pi^- \pi^+ \pi^+$. The muon and the two oppositely charged pions forming the K_S are indicated. The π^- is the ‘‘curler’’ track with momentum around 50 MeV.

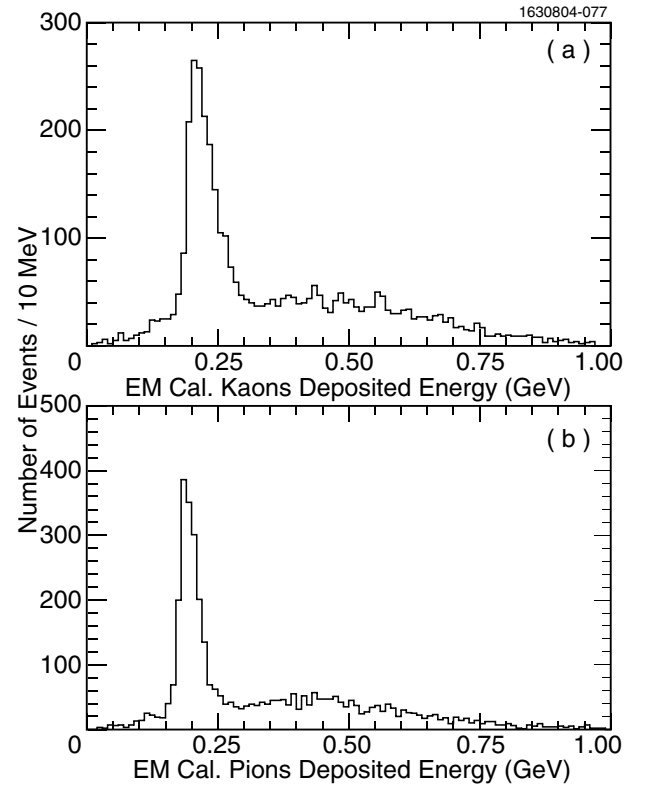


FIG. 9. Deposited energy in EM calorimeter for (a) kaons, (b) pions from $D^0 \rightarrow K^- \pi^+$.

TABLE IV. Backgrounds from specific D^+ decay modes.

Mode	\mathcal{B} (%)	No. of events
$\pi^+ \pi^0$	0.13 ± 0.02	0.31 ± 0.04
$\bar{K}^0 \pi^+$	2.77 ± 0.18	0.06 ± 0.05
$\tau^+ \nu$	$2.64 \times \mathcal{B}(D^+ \rightarrow \mu^+ \nu)$	0.30 ± 0.07
$\pi^0 \mu^+ \nu$	0.25 ± 0.15	Negligible
Sum		0.67 ± 0.09

0.06 events. We have simulated backgrounds from $D^+ \rightarrow \tau^+ \nu$. Out of 10 000 simulated events with D^- tags, we found background only when $\tau^+ \rightarrow \pi^+ \nu$. Because of the small $D^+ - \tau^+$ mass difference, the τ^+ is almost at rest in the laboratory frame and thus the π^+ has relatively large momentum causing the MM^2 distribution to populate only the low MM^2 region, even in this case with two missing neutrinos. The MM^2 distribution is shown in Fig. 11.

The semileptonic mode $\pi^0 \mu^+ \nu_\mu$ is similar to $\pi^+ \pi^0$ except that the π^0 often carries off enough momentum to result in large MM^2 . We found no candidate background events in a Monte Carlo sample consisting of 50 000 tags plus a $D^+ \rightarrow \pi^0 \mu^+ \nu$ decay.

C. $D^0 \bar{D}^0$ and continuum backgrounds

These backgrounds are evaluated by analyzing Monte Carlo samples corresponding to 5.2 times the total amount of data in our possession. To normalize our Monte Carlo events to our data sample we used $\sigma_{D^0 \bar{D}^0} = 3.5$ nb and $\sigma_{\text{continuum}} = 14.5$ nb [18]. In each sample we found one

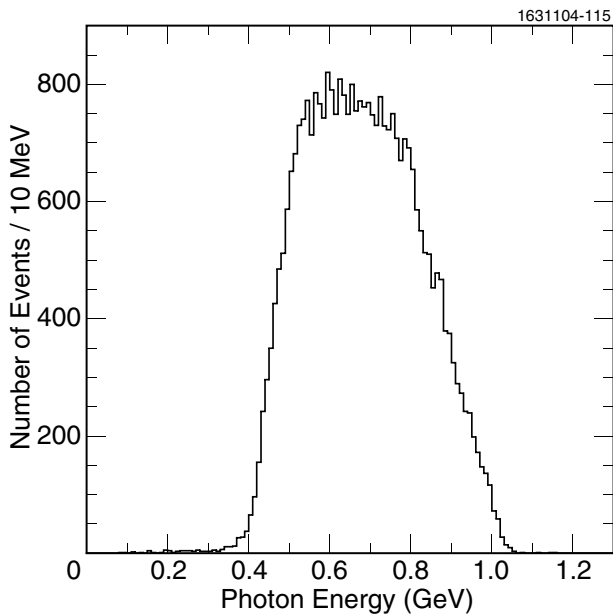


FIG. 10. Maximum photon energy in the $D^+ \rightarrow \pi^+ \pi^0$ decay from a GEANT simulation.

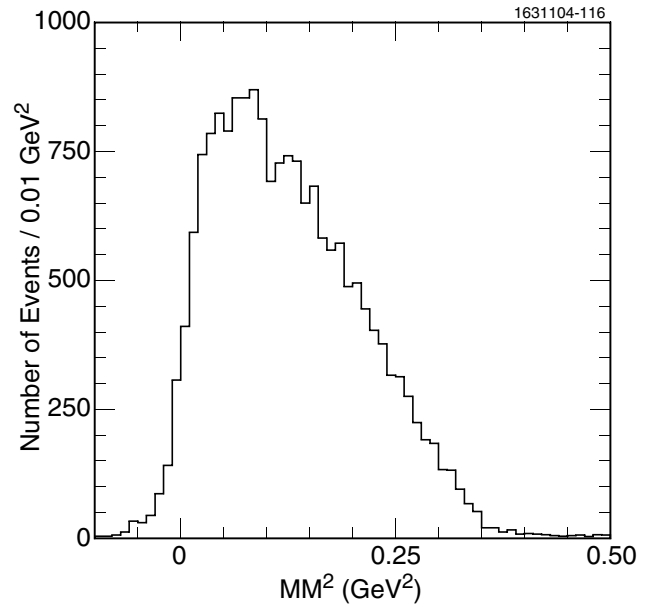


FIG. 11. Missing mass-squared distribution for $D^+ \rightarrow \tau^+ \nu$ and $\tau^+ \rightarrow \pi^+ \nu$.

background event within 2 standard deviations of zero. These correspond to 0.16 ± 0.16 $D^0 \bar{D}^0$ events and 0.17 ± 0.17 continuum events forming background. As a check on the continuum background we analyzed 23 pb^{-1} of continuum data taken a center-of-mass energy of 3670 MeV. We did not find any $D^+ \rightarrow \mu^+ \nu$ candidate events.

D. Background summary

Our total background is 1.00 ± 0.25 events. The probability of one background event fluctuating to eight or more signal events is only 10^{-5} , and even including the 0.25 event uncertainty in the background the signal has greater than 5 standard deviation significance. Because of the uncertainties in the Monte Carlo simulation we assign a 100% error to our background estimate: 1.0 ± 1.0 events, for the purpose of evaluating the branching ratio.

VII. BRANCHING RATIO AND DECAY CONSTANT

Subtracting the 1.0 event background from our eight events in the signal region, we determine a branching fraction using a detection efficiency for the single muon of 69.9%. This efficiency includes the selection on MM^2 within $\pm 2\sigma$ limits, the tracking, the particle identification, the probability of the crystal energy being less than 300 MeV, and the probability of not having another unmatched shower in the event with energy greater than 250 MeV. We assign a relative 5.3% error on this efficiency, the components of which are shown in Table V. We use a 3% systematic error on track finding found using the double tagged events and we estimate the error on the particle identification cut to be 1% from studies of D^{*+}

TABLE V. Systematic errors on the $D^+ \rightarrow \mu^+ \nu_\mu$ efficiency.

	Systematic error (%)
MC statistics	0.8
Track finding	3
cut	1
Minimum ionization cut	1
Extra showers cut	4
Total	5.3

TABLE VI. Theoretical predictions of f_{D^+} and $f_{D_s^+}/f_{D^+}$.

Model	f_{D^+} (MeV)	$f_{D_s^+}/f_{D^+}$
Lattice QCD (Fermilab and MILC) [2]	$225^{+11}_{-13} \pm 21$	$1.17 \pm 0.06 \pm 0.06$
Quenched lattice QCD (UKQCD) [3]	$210 \pm 10^{+17}_{-16}$	$1.13 \pm 0.02^{+0.04}_{-0.02}$
QCD spectral sum rules [5]	203 ± 20	1.15 ± 0.04
QCD sum rules [6]	195 ± 20	
Relativistic quark model [7]	243 ± 25	1.10
Potential model [4]	238	1.01
Isospin mass splittings [8]	262 ± 29	

decays in higher beam energy data. The error on the minimum ionization cut on the muon candidate in the calorimeter is 0.2% and discussed in detail in Sec. V. A 4% dominantly systematic error due to rejection of events with excess shower energy is assigned to the efficiency of this cut determined by using the $D^0 \bar{D}^0$ sample and also discussed in Sec. V.

To compute the branching ratio we use 7.0 ± 2.8 signal events divided by 69.9% and the 28 574 D^{\mp} tags. No other efficiencies enter. The systematic error on the branching fraction arises from the 5.3% systematic error on the efficiency, a 2.2% systematic error in the number of D^- tags and a 15.4% systematic error on the background. The total systematic error, evaluated by adding these contributions in quadrature, is 16.4%. Our result for the branching fraction is

$$\mathcal{B}(D^+ \rightarrow \mu^+ \nu_\mu) = (3.5 \pm 1.4 \pm 0.6) \times 10^{-4}. \quad (5)$$

The decay constant f_{D^+} is then obtained from Eq. (1) using 1.04 ps as the D^+ lifetime and 0.224 as $|V_{cd}|$ [10]. Our final result is

$$f_{D^+} = (202 \pm 41 \pm 17) \text{ MeV}. \quad (6)$$

VIII. CONCLUSIONS

There have been several experimental studies of D meson decay constants. The Mark III group published an upper limit of $\mathcal{B}(D^+ \rightarrow \mu^+ \nu_\mu) < 7.2 \times 10^{-4}$, which leads to an upper limit on the decay constant $f_{D^+} < 290$ MeV at 90% confidence level based on 9.3 pb^{-1} of data taken on the ψ'' [19]. BES claimed the observation of one event at a center-of-mass energy of 4.03 GeV with a

branching ratio of $(0.08^{+0.17}_{-0.05})\%$ [20]. Recently, using 33 pb^{-1} of ψ'' data they presented three event candidates with an estimated background of 0.33 events where neither $\pi^+ \pi^0$, or $\tau^+ \nu$ were mentioned as a possible background modes, nor was continuum background considered [21]. Here they find a branching ratio of $(0.122^{+0.111}_{-0.053} \pm 0.010)\%$, and a corresponding value of $f_{D^+} = (371^{+129}_{-119} \pm 25)$ MeV. Our value is considerably smaller, though compatible with their large error.

Our analysis shows the first statistically significant signal for $D^+ \rightarrow \mu^+ \nu$. The branching fraction is

$$\mathcal{B}(D^+ \rightarrow \mu^+ \nu) = (3.5 \pm 1.4 \pm 0.6) \times 10^{-4}, \quad (7)$$

and the decay constant is

$$f_{D^+} = (202 \pm 41 \pm 17) \text{ MeV}. \quad (8)$$

Our result for f_{D^+} , at the current level of precision, is consistent with predictions of lattice QCD and models listed in Table VI.

The models generally predict $f_{D_s^+}$ to be 10%–15% larger than f_{D^+} . CLEO previously measured $f_{D_s^+}$ as $(280 \pm 19 \pm 28 \pm 34)$ MeV [22], and we are consistent with these predictions as well. We look forward to more data to improve the precision.

ACKNOWLEDGMENTS

We gratefully acknowledge the effort of the CESR staff in providing us with excellent luminosity and running conditions. This work was supported by the National Science Foundation and the U.S. Department of Energy.

- [1] C. Davies *et al.*, Phys. Rev. Lett. **92**, 022001 (2004); C. Davies, in *Heavy Flavour Physics*, Scottish Graduate Textbook Series, edited by C.T.H. Davies and S.M. Playfer (Institute of Physics, Bristol, 2002); A. Kronfeld, Nucl. Phys. Proc. Suppl. **B129**, 46 (2004).
- [2] MILC Collaboration, J. Simone *et al.*, hep-lat/0410030 [Phys. Rev. Lett. (to be published)].
- [3] UKQCD Collaboration, L. Lellouch and C.-J. Lin, Phys. Rev. D **64**, 094501 (2001).
- [4] Z. G. Wang *et al.*, hep-ph/0403259; L. Salcedo *et al.*, Braz. J. Phys. **34**, 297 (2004).
- [5] S. Narison, hep-ph/0202200.
- [6] A. Penin and M. Steinhauser, Phys. Rev. D **65**, 054006 (2002).
- [7] D. Ebert *et al.*, Mod. Phys. Lett. A **17**, 803 (2002).
- [8] J. Amundson *et al.*, Phys. Rev. D **47**, 3059 (1993).
- [9] J.L. Rosner, in *Proceedings of the 1988 Banff Summer Institute, Banff, Alberta, Canada*, edited by A.N. Kamal and F.C. Khanna (World Scientific, Singapore, 1989), p. 395.
- [10] PDG Collaboration, S. Eidelman *et al.*, Phys. Lett. B **592**, 1 (2004).
- [11] Nonstandard models predict different ratios; see, for example, A.G. Akeroyd and S. Recksiegel, Phys. Lett. B **554**, 38 (2003).
- [12] D. Peterson *et al.*, Nucl. Instrum. Methods Phys. Res., Sect. A **478**, 142 (2002).
- [13] M. Artuso *et al.*, Nucl. Instrum. Methods Phys. Res., Sect. A **502**, 91 (2003).
- [14] CLEO Collaboration, Y. Kubota *et al.*, Nucl. Instrum. Methods Phys. Res., Sect. A **320**, 66 (1992).
- [15] The function is $f(m_D) = A(m_D + B) \times \sqrt{1 - \left(\frac{m_D + B}{C}\right)^2} e^{D\{1 - [(m_D + B)/C]^2\}}$. Here A is the overall normalization and B , C , and D are parameters that govern the shape. See ARGUS Collaboration, H. Albrecht *et al.*, Phys. Lett. B **229**, 304 (1989).
- [16] The tail appears to be caused by initial state radiation.
- [17] CLEO Collaboration, K. Arns *et al.*, Phys. Rev. D **69**, 071102 (2004).
- [18] CLEO Collaboration, B.I. Eisenstein *et al.*, hep-ex/0408055.
- [19] Mark III Collaboration, J. Adler *et al.*, Phys. Rev. Lett. **60**, 1375 (1988); **63**, 1658(E) (1989).
- [20] BES Collaboration, J.Z. Bai *et al.*, Phys. Lett. B **429**, 188 (1998).
- [21] BES Collaboration, M. Ablikim *et al.*, hep-ex/0410050.
- [22] CLEO Collaboration, M. Chadha *et al.*, Phys. Rev. D **58**, 032002 (1998).